UNIVERSITY OF LEEDS

This is a repository copy of *Computational studies of DNA base repair mechanisms by nonheme iron dioxygenases: selective epoxidation and hydroxylation pathways*.

White Rose Research Online URL for this paper:
https://eprints.whiterose.ac.uk/217680/

Version: Supplemental Material

Article:

Latifi, R., Minnick, J.L., Quesne, M.G. orcid.org/0000-0001-5130-1266 et al. (2 more authors) (2020) Computational studies of DNA base repair mechanisms by nonheme iron dioxygenases: selective epoxidation and hydroxylation pathways. Dalton Transactions, 49 (14). pp. 4266-4276. ISSN 1477-9226

https://doi.org/10.1039/d0dt00007h

© The Royal Society of Chemistry 2020. This is an author produced version of an article published in Dalton Transactions. Uploaded in accordance with the publisher's self-archiving policy.

Reuse
Items deposited in White Rose Research Online are protected by copyright, with all rights reserved unless indicated otherwise. They may be downloaded and/or printed for private study, or other acts as permitted by national copyright laws. The publisher or other rights holders may allow further reproduction and re-use of the full text version. This is indicated by the licence information on the White Rose Research Online record for the item.

Takedown
If you consider content in White Rose Research Online to be in breach of UK law, please notify us by emailing eprints@whiterose.ac.uk including the URL of the record and the reason for the withdrawal request.

White Rose
university consortium
Universities of Leeds, Sheffield & York

eprints@whiterose.ac.uk
https://eprints.whiterose.ac.uk/

Electronic Supporting Information

Computational studies of DNA base repair mechanisms by nonheme iron dioxygenases: Selective epoxidation and hydroxylation pathways

Reza Latifi,*[a] Jennifer L. Minnick,[a] Matthew G. Quesne,[b,c] Sam P. de Visser*[d] and Laleh Tahsini*[a]

a) 107 Physical Science Building, Department of Chemistry, Oklahoma State University, Stillwater, OK 74078, USA.
b) Cardiff University, School of Chemistry, Main Building, Park Place, Cardiff, CF10 3AT, United Kingdom.
c) Research Complex at Harwell, Rutherford Appleton Laboratory, Harwell Oxford, Didcot, Oxon, OX11 0FA, United Kingdom.
d) The Manchester Interdisciplinary Biocenter and the School of Chemical Engineering and Analytical Science, University of Manchester, 131 Princess Street, Manchester M1 7DN, United Kingdom.

QM/MM calculations

Table S1. Absolute energies (Hartree) for the minima structures in the oxygen activation path catalyzed by snapshot Sn$_{300}$. The superoxo (**Re$_{OO}$**), peracid (**Re$_{Cyc}$**) and ferryl oxo (**I$_{P}$**) intermediates are all shown alongside the single stable dioxygen species (**Re$_{OO}$***). The energies are broken down into separate MM and QM contributions as well as the combined total energies.

	QM$_{Turbomole}$	MM$_{DL\_poly}$	QMMM$_{Total}$
^{3}R$_{OO}$*	-3306.886852	-103.979836	-3410.866688
^{3}R$_{OO}$	-3306.89148	–103.986474	-3410.877954
^{5}R$_{OO}$	-3306.912856	–103.980312	-3410.893168
^{7}R$_{OO}$	-3306.913601	–103.980158	-3410.893759
^{3}Re$_{Cyc}$	-3306.94486	–103.993571	-3410.938431
^{5}Re$_{Cyc}$	-3306.965479	–104.001547	-3410.967026
^{7}Re$_{Cyc}$	-3306.896847	–103.983259	-3410.880106
^{3}I$_{P}$	-3306.963497	–103.995344	-3410.95884
^{5}I$_{P}$	-3306.976063	–103.999213	-3410.975276
^{7}I$_{P}$	-3306.98011	–103.978433	-3410.958543

Table S2. Absolute energies (Hartree) for the minima structures in the oxygen activation path catalyzed by snapshot Sn$_{400}$. The superoxo (**Re$_{OO}$**), peracid (**Re$_{Cyc}$**) and ferryl oxo (**I$_{P}$**) intermediates are all shown. The energies are broken down into separate MM and QM contributions as well as the combined total energies.

	QM$_{Turbomole}$	MM$_{DL\_poly}$	QMMM$_{Total}$
^{3}R$_{OO}$	-3306.953522	–103.765796	-3410.719318
^{5}R$_{OO}$	-3306.972756	–103.761067	-3410.733823
^{7}R$_{OO}$	-3306.973599	–103.761283	-3410.734882
^{3}Re$_{Cyc}$	-3307.002789	–103.777868	-3410.780657
^{5}Re$_{Cyc}$	-3307.021458	–103.77596	-3410.797417
^{7}Re$_{Cyc}$	-3306.964413	–103.760432	-3410.724846
^{3}I$_{P}$	-3307.050834	–103.754474	-3410.805308
^{5}I$_{P}$	-3307.062671	–103.752004	-3410.814675
^{7}I$_{P}$	-3306.985073	–103.722586	-3410.707659

Table S3. Absolute energies (Hartree) for the minima structures in the oxygen activation path catalyzed by snapshot Sn_{500}. The superoxo (**Re_{OO}**), peracid (**Re_{Cyc}**) and ferryl oxo (**I_P**) intermediates are all shown. The energies are broken down into separate MM and QM contributions as well as the combined total energies.

	$QM_{Turbomole}$	MM_{DL_poly}	$QMMM_{Total}$
$^{3}R_{OO}$	-3306.936762	–103.894914	-3410.831676
$^{5}R_{OO}$	-3306.973147	–103.870705	-3410.843852
$^{7}R_{OO}$	-3306.962929	–103.880245	-3410.843175
$^{3}Re_{Cyc}$	-3306.940199	–103.874952	-3410.815151
$^{5}Re_{Cyc}$	-3307.039706	–103.878672	-3410.918378
$^{7}Re_{Cyc}$	-3306.896832	–103.983277	-3410.880109
$^{3}I_P$	-3307.041241	–103.870006	-3410.911247
$^{5}I_P$	-3307.048999	–103.869045	-3410.918044
$^{7}I_P$	-3307.047534	–103.868693	-3410.916227

Table S4. Grouped spin populations for the minima structures in the oxygen activation path catalyzed by snapshot Sn_{300}. The superoxo (**Re_{OO}**), peracid (**Re_{Cyc}**) and ferryl oxo (**I_P**) intermediates are all shown alongside the single stable dioxygen species (**Re_{OO}***). The coordinating amino acids, iron co-factor as well as the distal (**O_1**) and proximal (**O_2**) oxygens of the bound dioxygen are all considered. The spin densities on the αKG co-enzyme is split into two groups for both the succinate (**suc**) and CO_2 components.

	Fe	**O_1**	**O_2**	**CO_2**	**suc**	**HIS_{131}**	**His_{187}**	**ARG**	**ASP**
$^{3}R_{OO}$*	3.67	-0.92	-0.93	0.06	0.01	0.04	0.05	-0.01	0.02
$^{3}R_{OO}$	2.98	-0.54	-0.62	0.07	0.04	-0.01	0.05	-0.01	0.05
$^{5}R_{OO}$	4.19	-0.30	-0.53	0.16	0.10	0.14	0.10	-0.01	0.16
$^{7}R_{OO}$	4.18	0.56	0.61	0.17	0.07	0.13	0.11	0.01	0.18
$^{3}Re_{Cyc}$	2.04	0.02	-0.02	0.01	-0.05	0.01	0.04	0.01	-0.06
$^{5}Re_{Cyc}$	3.75	0.06	0.01	0.00	0.03	0.07	0.03	0.00	0.04
$^{7}Re_{Cyc}$	4.29	0.20	0.12	0.52	0.49	0.12	0.10	0.00	0.15
$^{3}I_P$	2.84	-0.59	-0.24	0.01	-0.05	0.02	0.09	0.02	-0.10
$^{5}I_P$	4.21	-0.55	0.06	0.00	0.09	0.11	0.11	0.05	-0.08
$^{7}I_P$	4.20	1.01	0.32	0.01	0.12	0.08	0.12	0.00	0.15

Table S5. Grouped spin populations for the minima structures in the oxygen activation path catalyzed by snapshot Sn_{400}. The superoxo (**Re_{OO}**), peracid (**Re_{Cyc}**) and ferryl oxo (**I_P**) intermediates. The coordinating amino acids, iron co-factor as well as the distal (**O_1**) and proximal (**O_2**) oxygens of the bound dioxygen are all considered. The spin densities on the αKG co-enzyme is split into two groups for both the succinate (**suc**) and CO_2 components.

	Fe	**O_1**	**O_2**	**CO_2**	**suc**	**HIS_{131}**	**His_{187}**	**ARG**	**ASP**
$^{3}R_{OO}$	3.20	-0.66	-0.70	0.07	0.02	0.00	0.04	-0.01	0.03
$^{5}R_{OO}$	4.18	-0.30	-0.50	0.16	0.09	0.13	0.10	0.00	0.14
$^{7}R_{OO}$	4.17	0.61	0.61	0.14	0.06	0.12	0.11	0.01	0.17
$^{3}Re_{Cyc}$	1.99	0.05	-0.02	0.00	-0.05	0.03	0.04	0.00	-0.05
$^{5}Re_{Cyc}$	3.76	0.07	0.01	0.01	0.03	0.07	0.03	0.00	0.03
$^{7}Re_{Cyc}$	4.17	0.61	0.61	0.14	0.06	0.12	0.11	0.01	0.17
$^{3}I_P$	2.84	-0.59	-0.24	0.01	-0.05	0.02	0.09	0.02	-0.10
$^{5}I_P$	4.20	-0.54	0.02	0.00	0.10	0.13	0.12	0.05	-0.08
$^{7}I_P$	4.46	0.11	-0.01	0.93	0.25	0.10	0.04	0.04	0.06

Table S5. Grouped spin populations for the minima structures in the oxygen activation path catalyzed by snapshot Sn_{500}. The superoxo (**Re_{OO}**), peracid (**Re_{Cyc}**) and ferryl oxo (**I_P**) intermediates. The coordinating amino acids, iron co-factor as well as the distal (**O_1**) and proximal (**O_2**) oxygens of the bound dioxygen are all considered. The spin densities on the αKG co-enzyme is split into two groups for both the succinate (**suc**) and CO_2 components.

	Fe	**O_1**	**O_2**	**CO_2**	**suc**	**HIS_{131}**	**His_{187}**	**ARG**	**ASP**
$^{3}R_{OO}$	3.32	-0.76	-0.71	0.07	0.01	0.01	0.05	0.00	0.00
$^{5}R_{OO}$	4.19	-0.31	-0.52	0.18	0.07	0.13	0.09	-0.01	0.19
$^{7}R_{OO}$	4.18	0.52	0.64	0.15	0.07	0.12	0.10	0.01	0.20
$^{3}Re_{Cyc}$	1.12	0.05	0.09	0.44	0.35	0.00	-0.03	0.00	-0.02
$^{5}Re_{Cyc}$	3.76	0.06	0.01	0.01	0.02	0.07	0.03	0.00	0.04
$^{7}Re_{Cyc}$	4.32	0.16	0.09	0.55	0.49	0.12	0.09	0.00	0.16
$^{3}I_P$	1.37	0.63	0.04	0.00	-0.03	0.04	-0.03	0.00	-0.02
$^{5}I_P$	4.14	-0.29	-0.29	0.02	0.08	0.09	0.11	0.01	0.14
$^{7}I_P$	4.18	1.06	0.25	0.00	0.12	0.09	0.09	0.00	0.21

Table S6. Relative energies (kcal mol^{-1}) for the reaction landscape in the oxygen activation path catalyzed by snapshot $\mathrm{Sn_{300}}$. The superoxo (**$\mathrm{Re_{OO}}$**), peracid (**$\mathrm{Re_{Cyc}}$**) and ferryl oxo (**$\mathrm{I_P}$**) intermediates are all shown alongside the transition state for the initial attack of the superoxo on the beta carbon of the co-enzyme (**$\mathrm{TS_{O,C}}$**) and the barrier for the OO cleavage of the peracid (**$\mathrm{TS_{C,C}}$**). The energies are given for all possible spin states.

	S = 1	**S = 2**	**S = 3**
$\mathrm{R_{OO}}$	9.92	0.37	0.00
$\mathrm{TS_{O,C}}$	21.15	9.31	10.77
$\mathrm{Re_{Cyc}}$	-28.03	-45.98	8.57
$\mathrm{TS_{O,O}}$	-26.80	-41.26	24.25
$\mathrm{I_P}$	-40.84	-51.15	-40.65

Table S7. Relative energies (kcal mol^{-1}) for the reaction landscape in the oxygen activation path catalyzed by snapshot $\mathrm{Sn_{400}}$. The superoxo (**$\mathrm{Re_{OO}}$**), peracid (**$\mathrm{Re_{Cyc}}$**) and ferryl oxo (**$\mathrm{I_P}$**) intermediates are all shown alongside the transition state for the initial attack of the superoxo on the beta carbon of the co-enzyme (**$\mathrm{TS_{O,C}}$**) and the barrier for the OO cleavage of the peracid (**$\mathrm{TS_{C,C}}$**). The energies are given for all possible spin states.

Sn400	**S = 1**	**S = 2**	**S = 3**
$\mathrm{R_{OO}}$	9.77	0.66	0.00
$\mathrm{TS_{O,C}}$	19.68	13.53	13.14
$\mathrm{Re_{Cyc}}$	-28.72	-39.24	6.30
$\mathrm{TS_{O,O}}$	-19.98	-32.73	28.97
$\mathrm{I_P}$	-44.19	-50.07	17.08

Table S8. Relative energies (kcal mol^{-1}) for the reaction landscape in the oxygen activation path catalyzed by snapshot $\mathrm{Sn_{500}}$. The superoxo (**$\mathrm{Re_{OO}}$**), peracid (**$\mathrm{Re_{Cyc}}$**) and ferryl oxo (**$\mathrm{I_P}$**) intermediates are all shown alongside the transition state for the initial attack of the superoxo on the beta carbon of the co-enzyme (**$\mathrm{TS_{O,C}}$**) and the barrier for the OO cleavage of the peracid (**$\mathrm{TS_{C,C}}$**). The energies are given for all possible spin states.

Sn500	**S = 1**	**S = 2**	**S = 3**
$\mathrm{R_{OO}}$	7.22	-0.42	0.00
$\mathrm{TS_{O,C}}$	21.23	9.33	7.02
$\mathrm{Re_{Cyc}}$	17.59	-47.19	-23.18
$\mathrm{TS_{O,O}}$	24.22	-38.75	-7.49
$\mathrm{I_P}$	-42.72	-46.98	-45.84

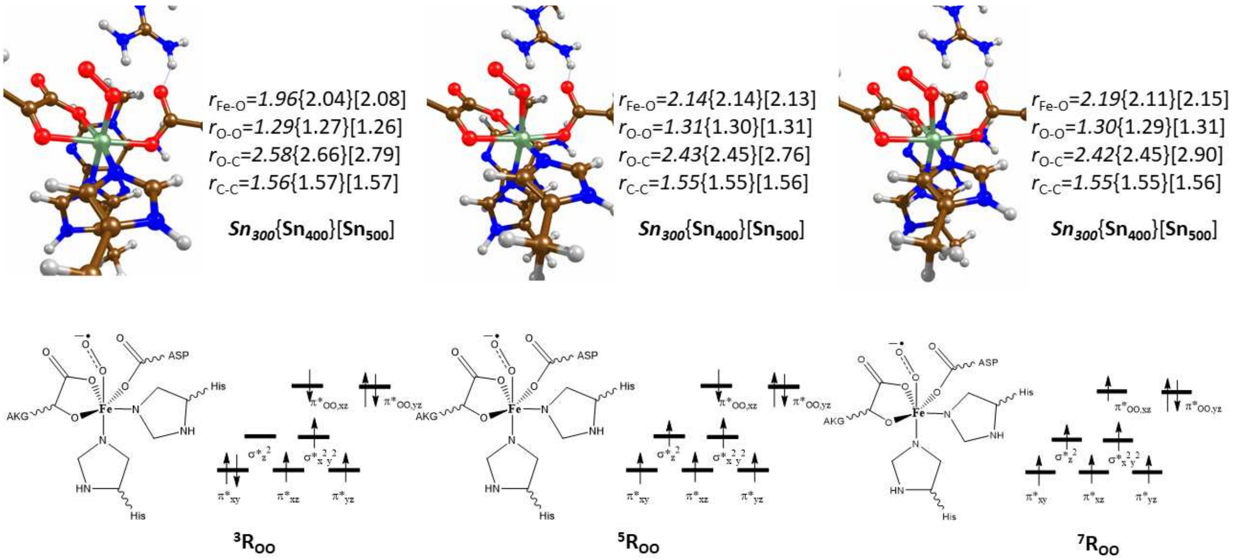

Fig. S1. Comparative orbital occupations and important bond lengths for the triplet (**^{3}Roo**), quintet (**^{5}Roo**) and septet (**^{7}Roo**) superoxo QM species.

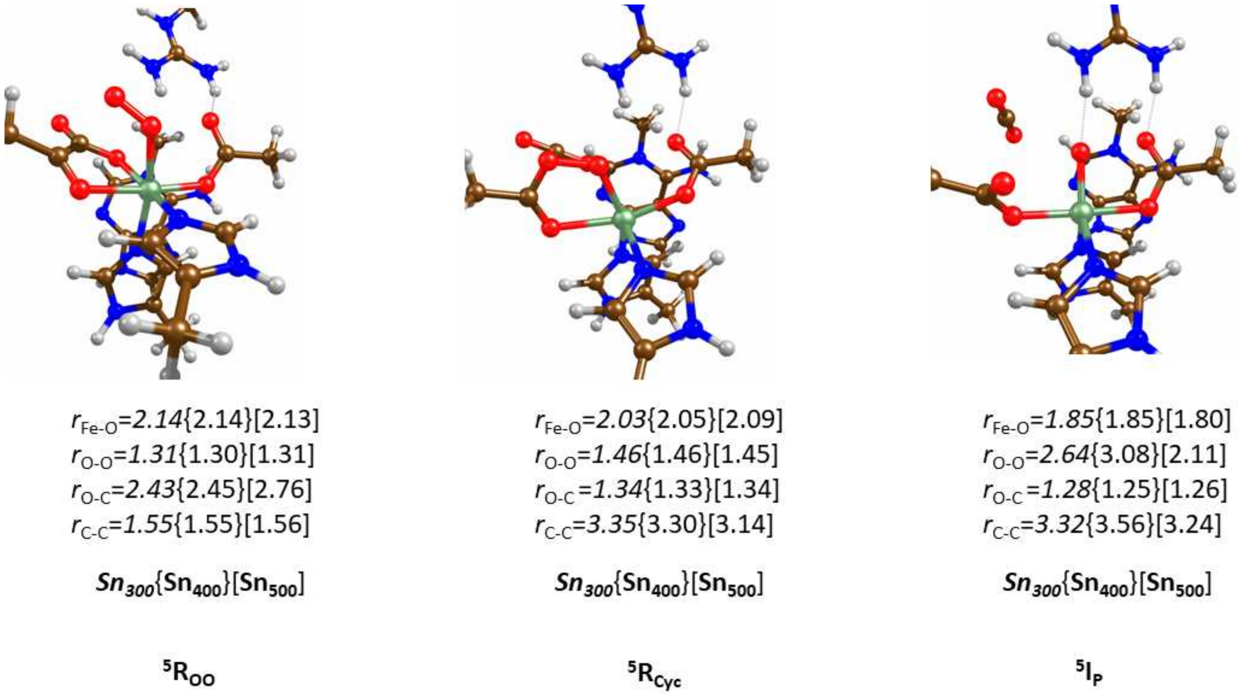

Fig. S2. Graphical representation of changes in the QM region at different minima point across the low energy quintet reaction pathways for oxygen activation. Important bond lengths for the superoxo (**^{5}Roo**), peracid (**^{5}R$_{Cyc}$**) and ferryl oxo (**^{5}I$_P$**) species are all shown.

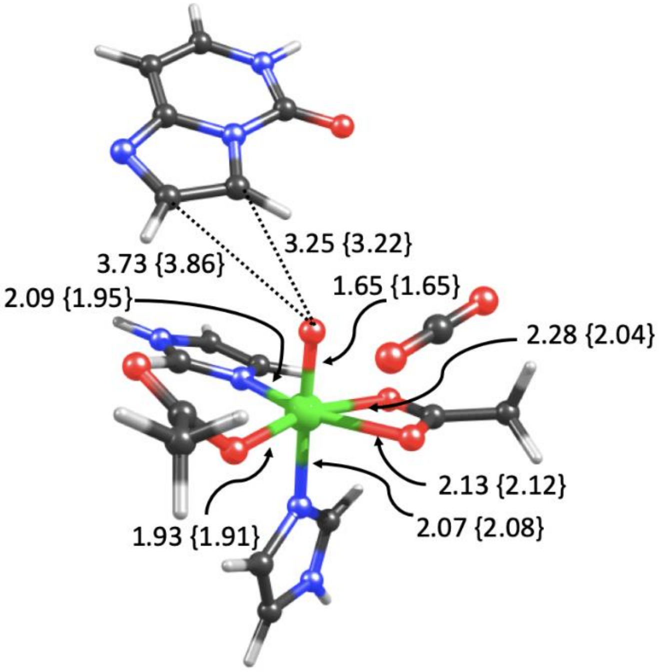

Fig. S3. Optimized geometries of ^{5}Re {^{3}R$_e$} for epoxidation reaction by iron(IV)-oxo species with alkylated Cytosine. All bond lengths are given in angstroms and the value of the imaginary frequency in the transition state in cm^{-1}.

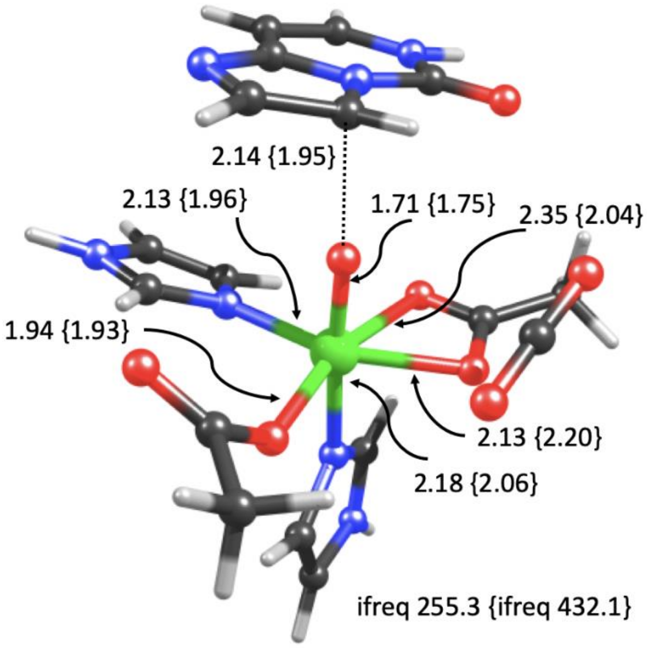

Fig. S4. Optimized geometries of ^{5}TS$_E$ {^{3}TS$_E$} for epoxidation reaction by iron(IV)-oxo species with alkylated Cytosine. All bond lengths are given in angstroms and the value of the imaginary frequency in the transition state in cm^{-1}.

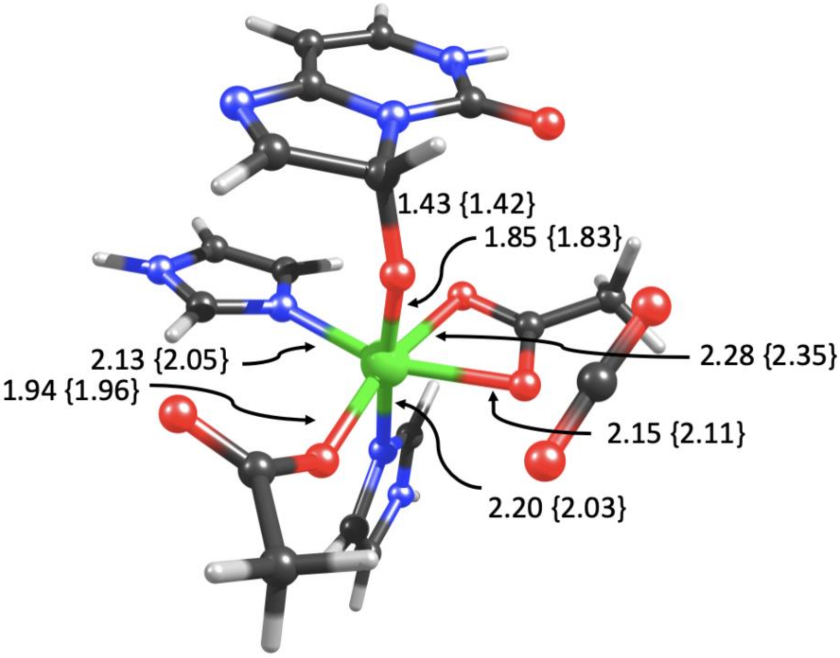

Fig. S5. Optimized geometries of $^{5}IM_{E}$ $\{^{3}IM_{E}\}$ for epoxidation reaction by iron(IV)-oxo species with alkylated Cytosine. All bond lengths are given in angstroms and the value of the imaginary frequency in the transition state in cm^{-1}.

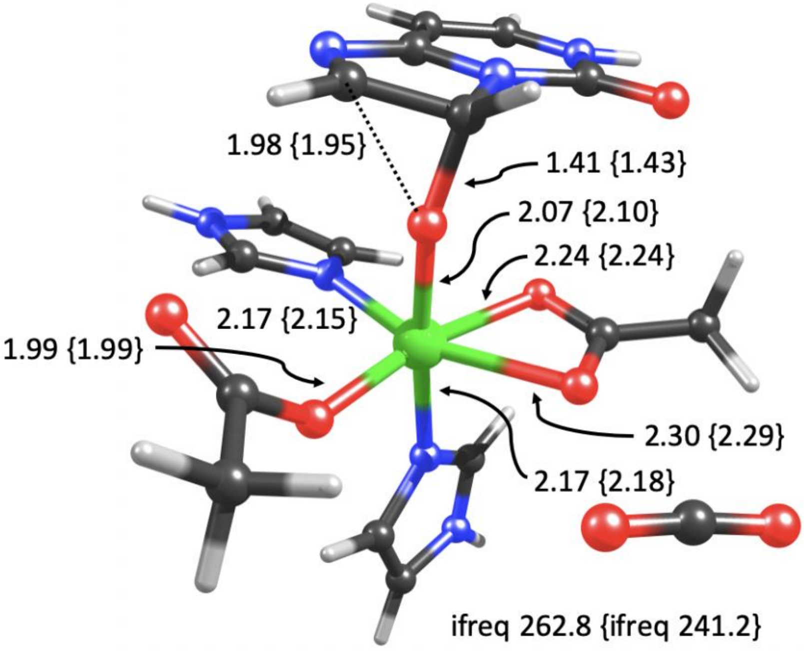

Fig. S6. Optimized geometries of $^{5}TS_{rc}$ $\{^{3}TS_{rc}\}$ for epoxidation reaction by iron(IV)-oxo species with alkylated Cytosine. All bond lengths are given in angstroms and the value of the imaginary frequency in the transition state in cm^{-1}.

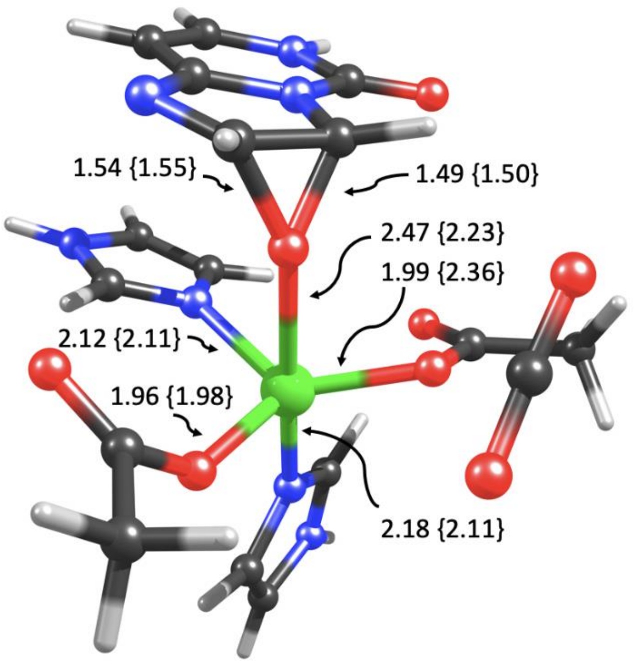

Fig. S7. Optimized geometries of ^5P_E {^3P_E} for epoxidation reaction by iron(IV)-oxo species with alkylated Cytosine. All bond lengths are given in angstroms and the value of the imaginary frequency in the transition state in cm^{-1}.

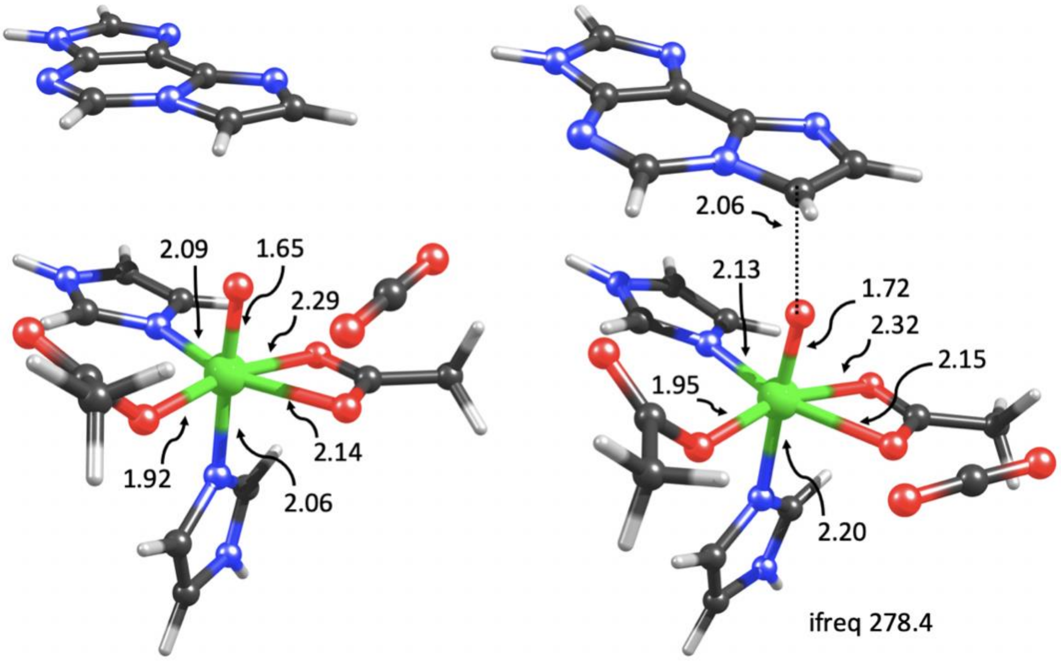

Fig. S8. Optimized geometries of ^{5}Re (left) and ^5TS_E (right) for epoxidation reaction by iron(IV)-oxo species with alkylated Adenine. All bond lengths are given in angstroms and the value of the imaginary frequency in the transition state in cm^{-1}.

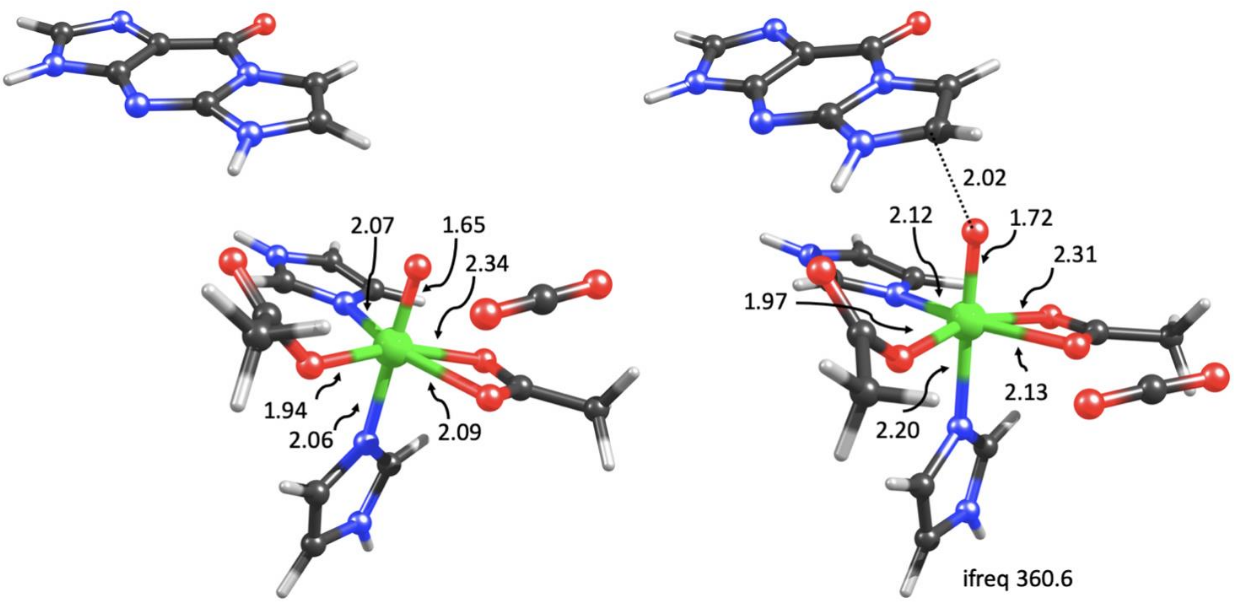

Fig. S9. Optimized geometries of ^{5}Re (left) and ^{5}TS$_{E}$ (right) for hydroxylation reaction by iron(IV)-oxo species with alkylated Guanine. All bond lengths are given in angstroms and the value of the imaginary frequency in the transition state in cm^{-1}.

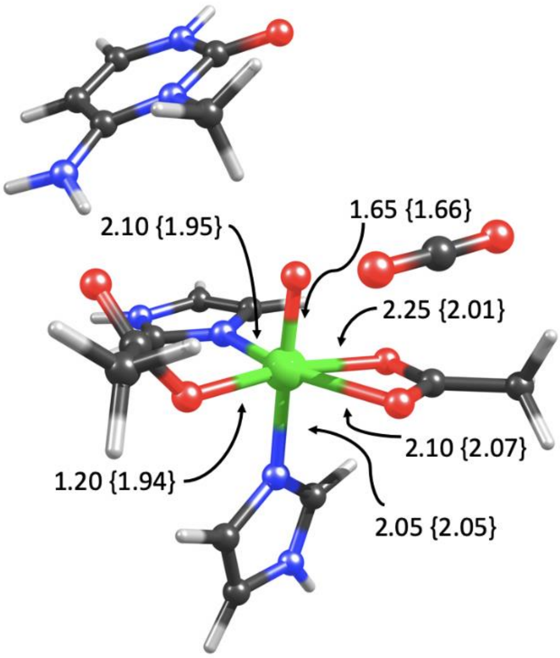

Fig. S10. Optimized geometries of ^{5}Re {^{3}Re} for hydroxylation reaction by iron(IV)-oxo species with alkylated Cytosine. All bond lengths are given in angstroms and the value of the imaginary frequency in the transition state in cm^{-1}.

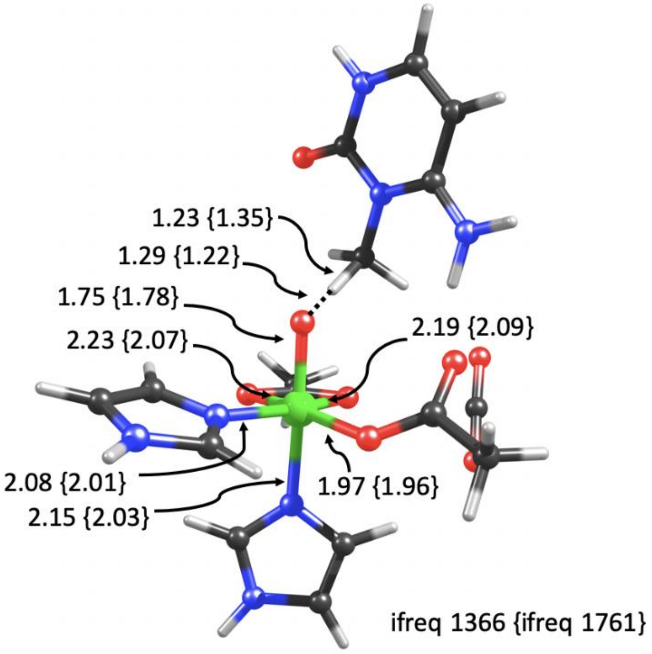

Fig. S11. Optimized geometries of $^{5}TS_{H}$ $\{^{3}TS_{H}\}$ for hydroxylation reaction by iron(IV)-oxo species with alkylated Cytosine. All bond lengths are given in angstroms and the value of the imaginary frequency in the transition state in cm⁻¹.

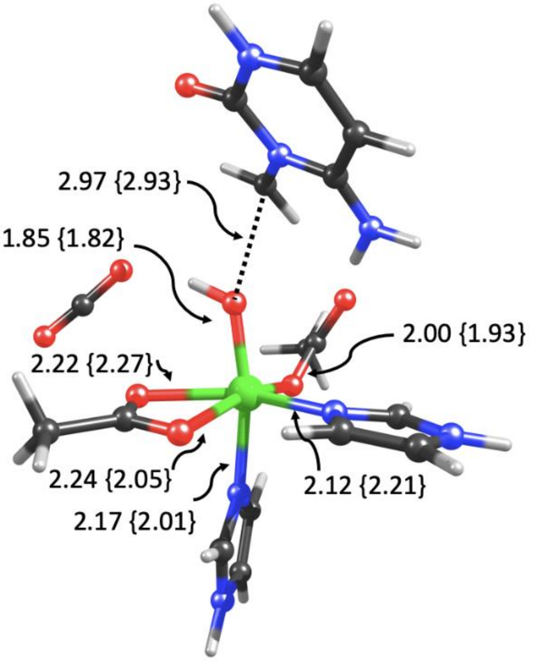

Fig. S12. Optimized geometries of $^{5}IM_{H}$ $\{^{3}IM_{H}\}$ for hydroxylation reaction by iron(IV)-oxo species with alkylated Cytosine. All bond lengths are given in angstroms and the value of the imaginary frequency in the transition state in cm⁻¹.

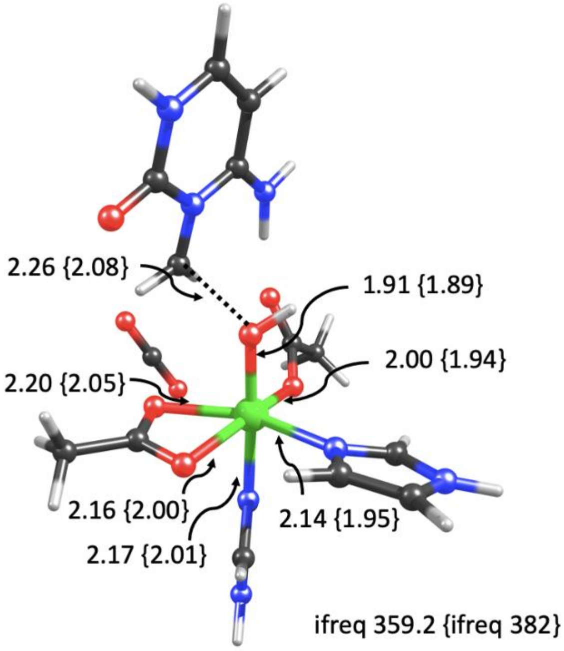

Fig. S13. Optimized geometries of $^5TS_{reb}$ $\{^3TS_{reb}\}$ for hydroxylation reaction by iron(IV)-oxo species with alkylated Cytosine. All bond lengths are given in angstroms and the value of the imaginary frequency in the transition state in cm^{-1}.

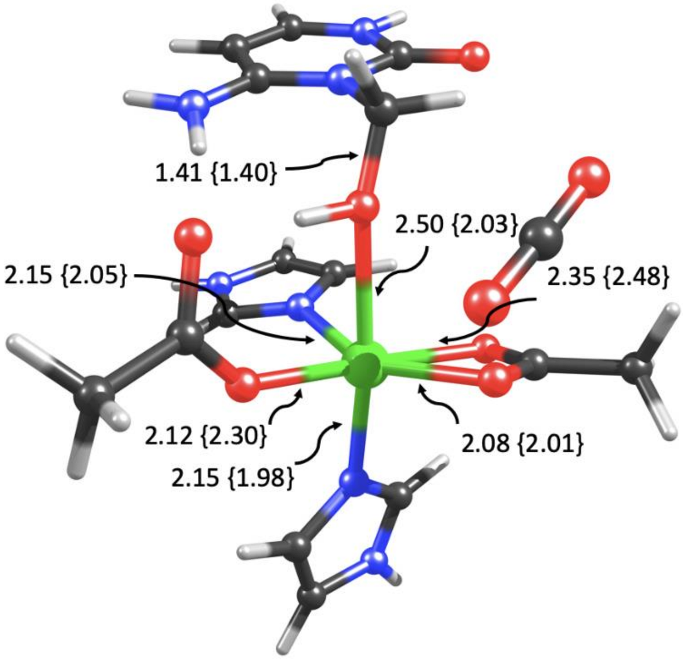

Fig. S14. Optimized geometries of ^5P_H $\{^3P_H\}$ for hydroxylation reaction by iron(IV)-oxo species with alkylated Cytosine. All bond lengths are given in angstroms and the value of the imaginary frequency in the transition state in cm^{-1}.

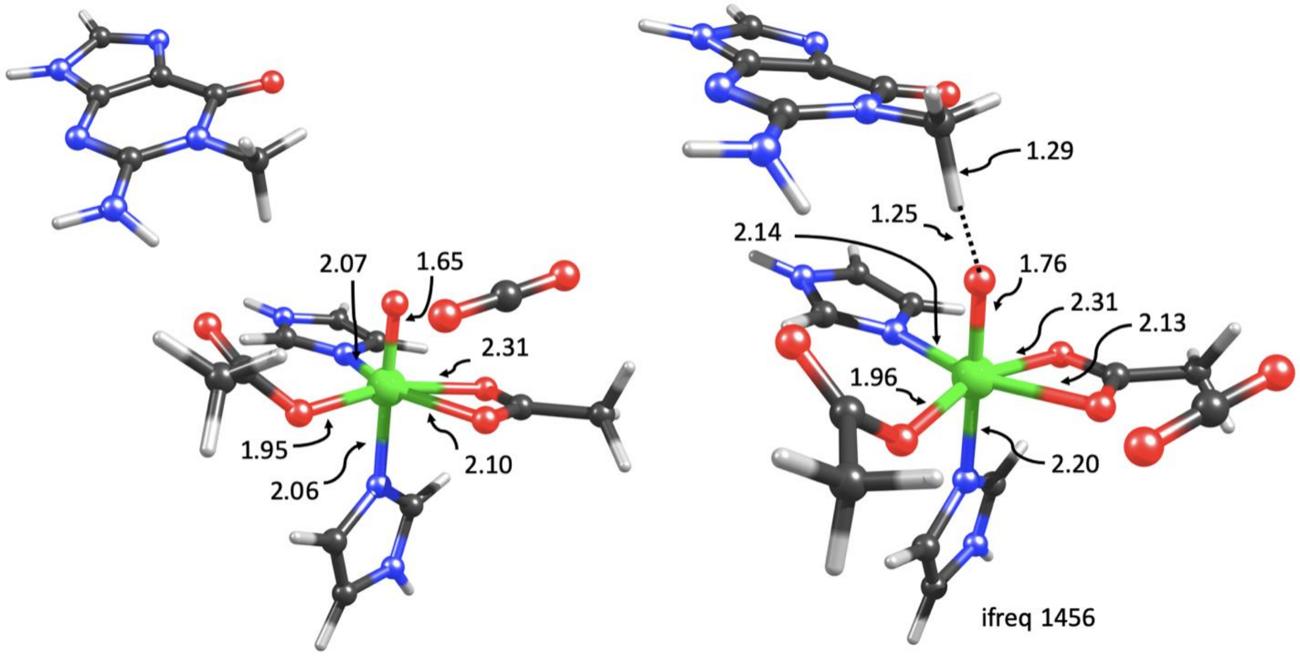

Fig. S15. Optimized geometries of ^{5}Re (left) and ^{5}TS$_H$ (right) for hydroxylation reaction by iron(IV)-oxo species with alkylated Guanine. All bond lengths are given in angstroms and the value of the imaginary frequency in the transition state in cm^{-1}.

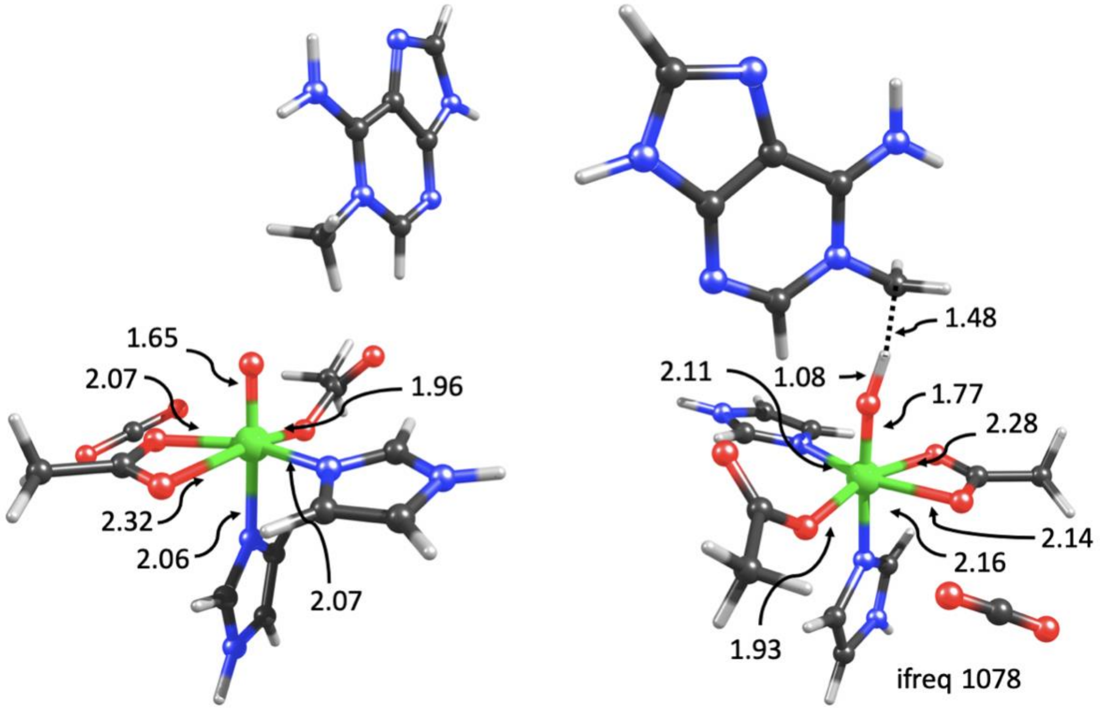

Fig. S16. Optimized geometries of ^{5}Re (left) and ^{5}TS$_H$ (right) for hydroxylation reaction by iron(IV)-oxo species with alkylated Adenine. All bond lengths are given in angstroms and the value of the imaginary frequency in the transition state in cm^{-1}.

Table S9. Absolute energies of all epoxidation structures described in this work.

	E (LACVP)	**ZPE**	**G**	**E (LACV3P+*)**
	(au)	(kcal/mol)	(au)	(au)
^{1}**Re**	-1767.570763	0.378753	-1767.2541	-1768.273169
^{3}**Re**	-1767.619247	0.379556	-1767.3014	-1768.323704
^{5}**Re**	-1767.628520	0.378162	-1767.3157	-1768.338381
^{7}**Re**	-1767.610836	0.376252	-1767.2989	-1768.319167
^{1}**TS$_{E}$**	-1767.563873	0.378413	-1767.2471	-1768.262860
^{3}**TS$_{E}$**	-1767.593207	0.378456	-1767.2764	-1768.293683
^{5}**TS$_{E}$**	-1767.613687	0.376397	-1767.3026	-1768.325039
^{7}**TS$_{E}$**	-1767.600822	0.375990	-1767.2902	-1768.311652
^{1}**IM$_{E}$**	-1767.591178	0.378735	-1767.2725	-1768.297585
^{3}**IM$_{E}$**	-1767.603585	0.377239	-1767.2852	-1768.312414
^{5}**IM$_{E}$**	-1767.614469	0.374670	-1767.3026	-1768.325723
^{7}**IM$_{E}$**	-1767.641175	0.376734	-1767.3297	-1768.358120
^{1}**TS$_{rc}$**	-1767.597769	0.378468	-1767.2799	-1768.309723
^{3}**TS$_{rc}$**	-1767.578468	0.374595	-1767.2913	-1768.300033
^{5}**TS$_{rc}$**	-1767.629027	0.375842	-1767.3190	-1768.349898
^{7}**TS$_{rc}$**	-1767.571735	0.374394	-1767.2691	-1768.287445
^{1}**P$_{E}$**	-1767.614656	0.380195	-1767.2947	-1768.328372
^{3}**P$_{E}$**	-1767.612720	0.378152	-1767.2960	-1768.331372
^{5}**P$_{E}$**	-1767.636257	0.376903	-1767.3246	-1768.359487
^{7}**P$_{E}$**	-1767.635387	0.375709	-1767.3220	-1768.356517

Table S10. Group spin densities and charges of optimized UB3LYP/B1 geometries in epoxidation reaction.

	ρ_{Fe}	$\rho_{Ligands}$	ρ_{O}	$\rho_{Cytosine}$	ρ_{Total}	Q_{Fe}	$Q_{Ligands}$	Q_{O}	$Q_{Cytosine}$	Q_{Total}
^{1}Re	0.69	-0.06	-0.64	0.00	0.00	0.62	-0.27	-0.33	-0.02	0.00
^{3}Re	1.10	-0.05	0.96	0.00	2.00	0.60	-0.25	-0.33	-0.02	0.00
^{5}Re	2.95	0.33	0.72	0.00	4.00	0.74	-0.39	-0.34	-0.02	0.00
^{7}Re	3.98	0.63	1.39	0.00	6.00	0.90	-0.51	-0.36	-0.03	0.00
^{1}TS$_{E}$	0.81	-0.05	-0.34	-0.41	0.00	0.67	-0.40	-0.45	0.18	0.00
^{3}TS$_{E}$	2.74	0.23	-0.52	-0.45	2.00	0.78	-0.55	-0.44	0.22	0.00
^{5}TS$_{E}$	3.64	0.40	0.22	-0.25	4.00	0.82	-0.56	-0.46	0.20	0.00
^{7}TS$_{E}$	3.98	0.54	1.16	0.32	6.00	0.86	-0.61	-0.47	0.21	0.00
^{1}IM$_{E}$	0.99	-0.06	-0.01	-0.93	0.00	0.71	-0.31	-0.57	0.17	0.00
^{3}IM$_{E}$	2.83	0.22	-0.09	-0.96	2.00	0.81	-0.49	-0.52	0.20	0.00
^{5}IM$_{E}$	4.02	0.56	0.30	-0.89	4.00	0.93	-0.56	-0.61	0.24	0.00
^{7}IM$_{E}$	4.04	0.60	0.36	1.01	6.00	0.93	-0.54	-0.60	0.21	0.00
^{1}TS$_{rc}$	-0.06	-0.01	-0.06	0.13	0.00	0.60	-0.70	-0.48	0.57	0.00
^{3}TS$_{rc}$	1.98	0.11	0.06	-0.15	2.00	0.69	-0.80	-0.47	0.59	0.00
^{5}TS$_{rc}$	3.81	0.27	0.11	-0.19	4.00	0.79	-0.84	-0.50	0.55	0.00
^{7}TS$_{rc}$	4.06	0.66	0.24	1.04	6.00	0.99	-0.49	-0.58	0.08	0.00
	ρ_{Fe}	$\rho_{Ligands}$	$\rho_{Product}$	ρ_{Total}		Q_{Fe}	$Q_{Ligands}$	$Q_{Product}$	Q_{Total}	
^{1}P$_{E}$	0.01	-0.01	0.00	0.00		0.58	-0.70	0.12	0.00	
^{3}P$_{E}$	1.95	0.04	0.01	2.00		0.67	-0.76	0.09	0.00	
^{5}P$_{E}$	3.74	0.25	0.01	4.00		0.83	-0.91	0.08	0.00	
^{7}P$_{E}$	4.03	0.59	1.38	6.00		0.93	-0.53	-0.40	0.00	

Table S11. Group spin densities and charges of single point UB3LYP/B2 calculations on UB3LYP/B1 optimized geometries for epoxidation reaction.

	ρ_{Fe}	$\rho_{Ligands}$	ρ_{O}	$\rho_{Cytosine}$	ρ_{Total}	Q_{Fe}	$Q_{Ligands}$	Q_{O}	$Q_{Cytosine}$	Q_{Total}
^{1}Re	0.70	-0.08	-0.61	0.00	0.00	0.62	-0.27	-0.33	-0.02	0.00
^{3}Re	1.16	-0.07	0.91	0.00	2.00	0.43	-0.21	-0.16	-0.06	0.00
^{5}Re	3.10	0.26	0.64	0.00	4.00	0.39	-0.21	-0.13	-0.05	0.00
^{7}Re	4.13	0.55	1.30	0.01	6.00	0.63	-0.42	-0.17	-0.04	0.00
^{1}TS$_E$	0.85	-0.07	-0.34	-0.44	0.00	0.62	-0.40	-0.21	-0.01	0.00
^{3}TS$_E$	2.81	0.18	-0.52	-0.47	2.00	0.70	-0.53	-0.19	0.02	0.00
^{5}TS$_E$	3.77	0.31	0.19	-0.27	4.00	0.59	-0.40	-0.21	0.01	0.00
^{7}TS$_E$	4.15	0.44	1.06	0.34	6.00	0.63	-0.44	-0.24	0.06	0.00
^{1}IM$_E$	1.03	-0.07	-0.01	-0.95	0.00	0.71	-0.34	-0.31	-0.05	0.00
^{3}IM$_E$	2.91	0.16	-0.10	-0.98	2.00	0.73	-0.44	-0.21	-0.07	0.00
^{5}IM$_E$	4.18	0.46	0.27	-0.91	4.00	0.77	-0.45	-0.34	0.01	0.00
^{7}IM$_E$	4.19	0.49	0.30	1.02	6.00	0.78	-0.42	-0.33	-0.03	0.00
^{1}TS$_{rc}$	-0.07	0.00	-0.06	0.13	0.00	0.67	-0.74	-0.22	0.29	0.00
^{3}TS$_{rc}$	2.01	0.09	0.05	-0.15	2.00	0.72	-0.83	-0.17	0.29	0.00
^{5}TS$_{rc}$	3.90	0.21	0.08	-0.19	4.00	0.75	-0.81	-0.21	0.27	0.00
^{7}TS$_{rc}$	4.22	0.55	0.18	1.05	6.00	0.76	-0.25	-0.19	-0.32	0.00
	ρ_{Fe}	$\rho_{Ligands}$	$\rho_{Product}$	ρ_{Total}		Q_{Fe}	$Q_{Ligands}$	$Q_{Product}$	Q_{Total}	
^{1}P$_E$	0.02	-0.01	0.00	0.00		0.67	-0.96	0.29	0.00	
^{3}P$_E$	1.97	0.02	0.01	2.00		0.77	-0.98	0.21	0.00	
^{5}P$_E$	3.81	0.20	-0.01	4.00		0.71	-0.81	0.10	0.00	
^{7}P$_E$	4.19	0.49	1.33	6.00		0.66	-0.35	-0.31	0.00	

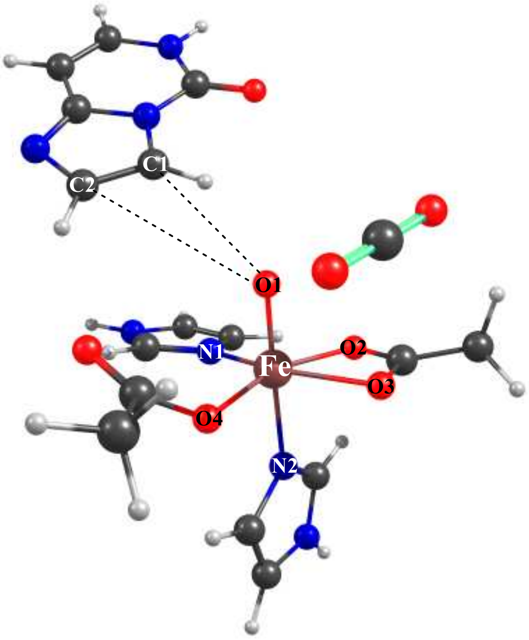

Table S12. All bond lengths in angstroms and obtained from geometry optimizations of epoxidation reaction in Gaussian at UB3LYP/B1.

	Fe-O1	**Fe-O2**	**Fe-O3**	**Fe-O4**	**Fe-N1**	**Fe-N2**	**O1-C1**	**O1-C2**
^{1}Re	1.70326	2.03158	2.11876	1.91060	1.95118	2.06322	3.20627	3.77641
^{3}Re	1.65250	2.04223	2.12473	1.91493	1.94702	2.07739	3.22303	3.85795
^{5}Re	1.64927	2.28205	2.13275	1.92770	2.08712	2.06879	3.25171	3.72760
^{7}Re	1.93592	2.36542	2.09256	1.93098	2.10234	2.17470	3.14594	3.85191
^{1}TS$_{E}$	1.75394	2.02674	2.20290	1.92225	1.94070	2.06782	1.92903	2.64566
^{3}TS$_{E}$	1.74732	2.03843	2.20072	1.93351	1.96169	2.06530	1.94638	2.67336
^{5}TS$_{E}$	1.71244	2.34825	2.13294	1.93837	2.12598	2.17696	2.13794	2.69638
^{7}TS$_{E}$	1.90480	2.31095	2.15125	1.94079	2.12895	2.22071	2.17446	2.64522
^{1}IM$_{E}$	1.85849	2.00346	2.12077	1.92395	1.96246	2.02423	1.40860	2.49953
^{3}IM$_{E}$	1.83218	2.36369	2.10034	1.96216	2.04779	2.02685	1.42300	2.50641
^{5}IM$_{E}$	1.84631	2.27555	2.15312	1.93699	2.12654	2.20339	1.42733	2.42206
^{7}IM$_{E}$	1.86934	2.28904	2.14956	1.92761	2.12566	2.19918	1.40732	2.42821
^{1}TS$_{rc}$	1.95220	2.10382	2.20286	2.00338	2.01417	1.98017	1.41033	2.00160
^{3}TS$_{rc}$	2.09999	2.24175	2.28532	1.98509	2.14590	2.16792	1.43155	1.94618
^{5}TS$_{rc}$	2.06541	2.24247	2.29726	1.98792	2.17221	2.17405	1.41456	1.98448
^{7}TS$_{rc}$	1.95048	2.27279	2.12851	1.91125	2.08059	2.15916	1.52640	1.65565
^{1}P$_{E}$	2.07269	2.09819	2.23115	2.00605	2.02209	2.00096	1.50436	1.56659
^{3}P$_{E}$	2.23910	2.03463	2.36329	1.98382	2.11388	2.10897	1.49577	1.55259
^{5}P$_{E}$	2.47254	3.17129	1.98886	1.95923	2.12496	2.17782	1.48550	1.54077
^{7}P$_{E}$	1.85611	2.28069	2.13706	1.92048	2.14957	2.21130	1.40689	2.43387

Table S13. Absolute energies of all structures described in this work for hydroxylation reaction.

	E (LACVP) (au)	**ZPE** (kcal/mol)	**G** (au)	**E (LACV3P+*)** (au)
$^{1}\mathbf{Re}$	-1731.101759	0.408898	-1730.7538	-1731.771229
$^{3}\mathbf{Re}$	-1731.164160	0.410127	-1730.8191	-1731.833125
$^{5}\mathbf{Re}$	-1731.172770	0.408783	-1730.8268	-1731.847229
$^{7}\mathbf{Re}$	-1731.165185	0.407189	-1730.8238	-1731.837261
$^{1}\mathbf{TS}_{\mathbf{H}}$	-1731.112278	0.403607	-1730.7723	-1731.772673
$^{3}\mathbf{TS}_{\mathbf{H}}$	-1731.150624	0.403076	-1730.8109	-1731.813370
$^{5}\mathbf{TS}_{\mathbf{H}}$	-1731.157975	0.402022	-1730.8192	-1731.829716
$^{7}\mathbf{TS}_{\mathbf{H}}$	-1731.138744	0.400981	-1730.7990	-1731.808883
$^{1}\mathbf{IM}_{\mathbf{H}}$	-1731.101672	0.407345	-1730.7552	-1731.771548
$^{3}\mathbf{IM}_{\mathbf{H}}$	-1731.132768	0.405389	-1730.7929	-1731.810758
$^{5}\mathbf{IM}_{\mathbf{H}}$	-1731.151604	0.403100	-1730.8098	-1731.825897
$^{7}\mathbf{IM}_{\mathbf{H}}$	-1731.153942	0.403609	-1730.8150	-1731.838528
$^{1}\mathbf{TS}_{\mathbf{reb}}$	-1731.149271	0.408708	-1730.7989	-1731.814160
$^{3}\mathbf{TS}_{\mathbf{reb}}$	-1731.164602	0.407192	-1730.8266	-1731.827744
$^{5}\mathbf{TS}_{\mathbf{reb}}$	-1731.160190	0.403187	-1730.8197	-1731.832007
$^{7}\mathbf{TS}_{\mathbf{reb}}$	-1731.164979	0.405386	-1730.8240	-1731.846534
$^{1}\mathbf{P}_{\mathbf{H}}$	-1731.214112	0.411702	-1730.8631	-1731.884443
$^{3}\mathbf{P}_{\mathbf{H}}$	-1731.211195	0.409730	-1730.8606	-1731.880578
$^{5}\mathbf{P}_{\mathbf{H}}$	-1731.234052	0.408664	-1730.8951	-1731.915444
$^{7}\mathbf{P}_{\mathbf{H}}$	-1731.169729	0.406679	-1730.8229	-1731.851548

Table S14. Group spin densities and charges of optimized UB3LYP/B1 geometries for hydroxylation reaction in Gaussian.

	ρ_{Fe}	$\rho_{Ligands}$	ρ_{O}	ρ_{ACH3}	ρ_{Total}	Q_{Fe}	$Q_{Ligands}$	Q_{O}	Q_{ACH3}	Q_{Total}
^{1}Re	0.80	-0.08	-0.72	0.00	0.00	0.61	-0.18	-0.38	0.94	1.00
^{3}Re	1.10	-0.06	0.95	0.00	2.00	0.59	-0.10	-0.34	0.85	1.00
^{5}Re	2.99	0.32	0.69	0.00	4.00	0.75	-0.25	-0.37	0.87	1.00
^{7}Re	3.99	0.64	1.37	0.00	6.00	0.90	-0.46	-0.37	0.93	1.00
	ρ_{Fe}	$\rho_{Ligands}$	ρ_{OH}	ρ_{ACH2}	ρ_{Total}	Q_{Fe}	$Q_{Ligands}$	Q_{OH}	Q_{ACH2}	Q_{Total}
^{1}TS$_{H}$	0.80	-0.04	-0.37	-0.39	0.00	0.57	-0.09	-0.11	0.63	1.00
^{3}TS$_{H}$	2.77	0.21	-0.51	-0.48	2.00	0.72	-0.28	-0.12	0.68	1.00
^{5}TS$_{H}$	3.70	0.41	0.15	-0.26	4.00	0.83	-0.33	-0.16	0.65	1.00
^{7}TS$_{H}$	4.05	0.56	0.84	0.55	6.00	0.87	-0.40	-0.19	0.72	1.00
^{1}IM$_{H}$	0.94	-0.06	0.10	-0.98	0.00	0.63	-0.14	-0.31	0.82	1.00
^{3}IM$_{H}$	2.02	0.16	0.03	-0.21	2.00	0.72	-0.26	-0.29	0.83	1.00
^{5}IM$_{H}$	4.05	0.53	0.40	-0.98	4.00	0.91	-0.44	-0.31	0.84	1.00
^{7}IM$_{H}$	4.06	0.58	0.37	0.99	6.00	0.90	-0.40	-0.36	0.86	1.00
^{1}TS$_{reb}$	0.85	-0.05	0.03	-0.84	0.00	0.60	-0.12	-0.23	0.75	1.00
^{3}TS$_{reb}$	2.55	0.18	0.00	-0.74	2.00	0.73	-0.32	-0.22	0.81	1.00
^{5}TS$_{reb}$	4.03	0.48	0.27	-0.78	4.00	0.87	-0.44	-0.30	0.87	1.00
^{7}TS$_{reb}$	4.11	0.69	0.23	0.96	6.00	0.95	-0.24	-0.25	0.53	1.00
	ρ_{Fe}	$\rho_{Ligands}$	ρ_{ACH2}	ρ_{Total}		Q_{Fe}	$Q_{Ligands}$	Q_{ACH2}	Q_{Total}	
^{1}P$_{H}$	0.00	0.00	0.00	0.00		0.54	-0.44	0.91	1.00	
^{3}P$_{H}$	1.98	0.03	-0.01	2.00		0.63	-0.54	0.92	1.00	
^{5}P$_{H}$	3.96	0.04	0.01	4.00		0.76	-0.63	0.87	1.00	
^{7}P$_{H}$	4.09	0.81	1.10	6.00		1.05	-0.24	0.19	1.00	

Table S15. Group spin densities and charges of single point UB3LYP/B2 calculations on UB3LYP/B1 optimized geometries for hydroxylation reaction in Gaussian.

	ρ_{Fe}	$\rho_{Ligands}$	ρ_{O}	ρ_{ACH3}	ρ_{Total}	Q_{Fe}	$Q_{Ligands}$	Q_{O}	Q_{ACH3}	Q_{Total}
^{1}Re	0.80	-0.10	-0.70	0.00	0.00	0.51	-0.21	-0.24	0.95	1.00
^{3}Re	1.17	-0.07	0.90	0.00	2.00	0.45	-0.14	-0.23	0.92	1.00
^{5}Re	3.13	0.24	0.63	0.00	4.00	0.48	-0.18	-0.22	0.92	1.00
^{7}Re	4.15	0.56	1.29	0.01	6.00	0.62	-0.37	-0.19	0.94	1.00
	ρ_{Fe}	$\rho_{Ligands}$	ρ_{OH}	ρ_{ACH2}	ρ_{Total}	Q_{Fe}	$Q_{Ligands}$	Q_{OH}	Q_{ACH2}	Q_{Total}
^{1}TS$_{H}$	0.83	-0.06	-0.38	-0.40	0.00	0.51	-0.20	0.18	0.52	1.00
^{3}TS$_{H}$	2.84	0.16	-0.51	-0.49	2.00	0.61	-0.37	0.19	0.58	1.00
^{5}TS$_{H}$	3.83	0.32	0.10	-0.25	4.00	0.62	-0.32	0.18	0.52	1.00
^{7}TS$_{H}$	4.21	0.48	0.77	0.55	6.00	0.70	-0.41	0.10	0.62	1.00
	4.21	0.47	0.75	0.57	6.00	0.69	-0.41	0.10	0.63	1.00
^{1}IM$_{H}$	0.97	-0.07	0.10	-0.99	0.00	0.56	-0.17	-0.24	0.85	1.00
^{3}IM$_{H}$	2.80	0.16	0.03	-0.99	2.00	0.72	-0.26	-0.29	0.83	1.00
^{5}IM$_{H}$	4.21	0.44	0.34	-0.99	4.00	0.86	-0.40	-0.29	0.83	1.00
^{7}IM$_{H}$	4.21	0.48	0.32	0.99	6.00	0.75	-0.39	-0.25	0.88	1.00
^{1}TS$_{reb}$	0.89	-0.06	0.04	-0.86	0.00	0.59	-0.27	-0.01	0.69	1.00
^{3}TS$_{reb}$	2.65	0.15	-0.01	-0.79	2.00	0.72	-0.44	0.01	0.70	1.00
^{5}TS$_{reb}$	4.17	0.40	0.24	-0.81	4.00	0.76	-0.44	-0.01	0.69	1.00
^{7}TS$_{reb}$	4.26	0.58	0.18	0.98	6.00	0.75	-0.19	0.01	0.43	1.00
	ρ_{Fe}	$\rho_{Ligands}$	ρ_{ACH2}	ρ_{Total}		Q_{Fe}	$Q_{Ligands}$	Q_{ACH2}	Q_{Total}	
^{1}P$_{H}$	0.00	0.00	0.00	0.00		0.54	-0.48	0.96	1.00	
^{3}P$_{H}$	2.03	-0.01	-0.02	2.00		0.53	-0.49	0.97	1.00	
^{5}P$_{H}$	3.84	0.17	-0.01	4.00		0.55	-0.50	0.95	1.00	
^{7}P$_{H}$	4.24	0.69	1.07	6.00		0.83	-0.24	0.41	1.00	

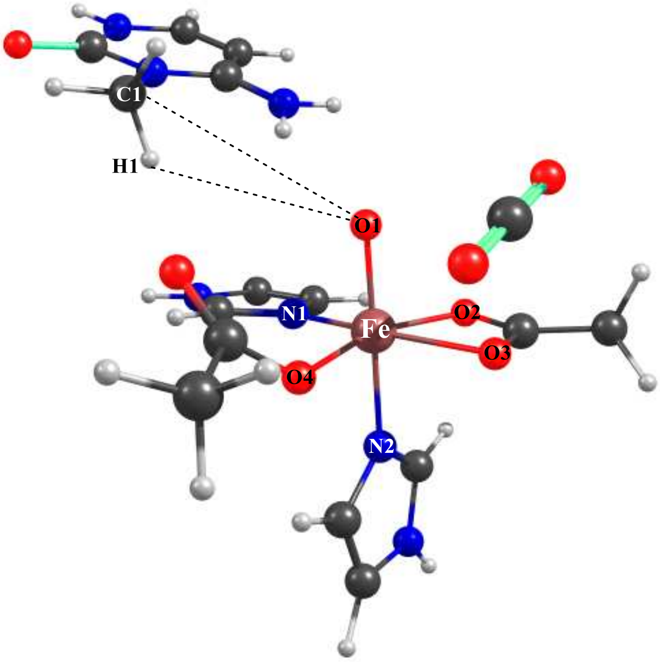

Table S16. All bond lengths in angstroms and obtained from geometry optimizations for hydroxylation reaction in Gaussian at UB3LYP/B1.

	Fe-O1	Fe-O2	Fe-O3	Fe-O4	Fe-N1	Fe-N2	O1-H1	H1-C1	O1-C1
$^{1}\mathrm{Re}$	1.74346	2.04614	2.04915	1.89882	1.95509	2.04803	3.61496	1.09283	4.33017
$^{3}\mathrm{Re}$	1.65568	2.01445	2.07153	1.93670	1.94867	2.05294	1.99734	1.09495	3.08993
$^{5}\mathrm{Re}$	1.64995	2.24744	2.09589	1.95733	2.10113	2.04743	1.95870	1.09415	3.02665
$^{7}\mathrm{Re}$	1.94090	2.33657	2.07411	1.94135	2.12006	2.16562	2.15901	1.09244	3.09906
$^{1}\mathrm{TS}_{\mathrm{H}}$	1.75326	2.01858	2.05638	1.91737	1.95000	2.02665	1.24603	1.34004	2.58562
$^{3}\mathrm{TS}_{\mathrm{H}}$	1.78251	2.07040	2.09459	1.95991	2.00576	2.02952	1.22450	1.35370	2.57795
$^{5}\mathrm{TS}_{\mathrm{H}}$	1.74556	2.23539	2.18663	1.97444	2.08353	2.14612	1.29417	1.22925	2.51828
$^{7}\mathrm{TS}_{\mathrm{H}}$	1.85239	2.08668	2.10592	1.95619	2.01861	2.08723	1.22147	1.34324	2.56216
$^{1}\mathrm{IM}_{\mathrm{H}}$	1.82031	2.03036	2.03170	1.93958	1.97078	2.02285	0.98036	3.15281	2.96202
$^{3}\mathrm{IM}_{\mathrm{H}}$	1.81880	2.05400	2.27944	1.92551	2.20514	2.01088	0.98228	3.13086	2.92549
$^{5}\mathrm{IM}_{\mathrm{H}}$	1.84838	2.24262	2.21821	2.00466	2.11811	2.17147	0.97954	2.82545	2.97008
$^{7}\mathrm{IM}_{\mathrm{H}}$	1.86324	2.33383	2.14215	1.94260	2.21081	2.15754	0.97596	3.02486	2.99143
$^{1}\mathrm{TS}_{\mathrm{reb}}$	1.85981	2.00575	2.04344	1.94203	1.95857	2.00445	0.98062	2.54284	2.12298
$^{3}\mathrm{TS}_{\mathrm{reb}}$	1.88607	1.99570	2.04713	1.93758	1.95466	2.01450	0.98210	2.50770	2.07661
$^{5}\mathrm{TS}_{\mathrm{reb}}$	1.90647	2.20376	2.16335	1.99757	2.14106	2.16942	0.97729	2.68542	2.26828
$^{7}\mathrm{TS}_{\mathrm{reb}}$	1.98228	2.16661	2.18238	1.96483	2.08898	2.14868	0.99887	2.24911	1.80415
$^{1}\mathrm{P}_{\mathrm{H}}$	2.03055	2.07331	2.09276	2.09422	1.99724	1.98202	1.06698	2.10221	1.39730
$^{3}\mathrm{P}_{\mathrm{H}}$	2.02596	2.47652	2.01485	2.29901	2.05438	1.98025	1.08950	2.13458	1.40241
$^{5}\mathrm{P}_{\mathrm{H}}$	2.50446	2.35400	2.07597	2.11548	2.14701	2.14738	1.02155	2.02381	1.41016
$^{7}\mathrm{P}_{\mathrm{H}}$	2.07470	2.24636	2.15561	1.89127	2.08590	2.11389	0.98337	2.04671	1.50046